THE ASTROPHYSICAL JOURNAL
Preprint typeset using LaTeX style emulateapj v. 01/23/15

arXiv:1606.09316v2 [astro-ph.HE] 15 Sep 2016

SUPERNOVAE POWERED BY MAGNETARS THAT TRANSFORM INTO BLACK HOLES

TAKASHI J. MORIYA
Division of Theoretical Astronomy, National Astronomical Observatory of Japan, National Institues of Natural Sciences,
2-21-1 Osawa, Mitaka, Tokyo 181-8588, Japan
takashi.moriya@nao.ac.jp

BRIAN D. METZGER
Columbia Astrophysics Laboratory, Columbia University, New York, NY 10027, USA

SERGEI I. BLINNIKOV
Institute for Theoretical and Experimental Physics, Bolshaya Cheremushkinskaya ulitsa 25, 117218 Moscow, Russia
All-Russia Research Institute of Automatics, Sushchevskaya ulitsa 22, 127055 Moscow, Russia and
Kavli Institute for the Physics and Mathematics of the Universe (WPI), The University of Tokyo Institutes for Advanced Study, The University of Tokyo,
5-1-5 Kashiwanoha, Kashiwa 277-8583, Japan

Received 2016 June 29; revised 2016 September 14; accepted 2016 September 15

ABSTRACT

Rapidly rotating, strongly magnetized neutron stars (magnetars) can release their enormous rotational energy via magnetic spin-down, providing a power source for bright transients such as superluminous supernovae. On the other hand, particularly massive (so-called supramassive) neutron stars require a minimum rotation rate to support their mass against gravitational collapse, below which the neutron star collapses to a black hole. We model the light curves of supernovae powered by magnetars which transform into black holes. Although the peak luminosities can reach high values in the range of superluminous supernovae, their post maximum light curves can decline very rapidly because of the sudden loss of the central energy input. Early black hole transformation also enhances the shock breakout signal from the magnetar-driven bubble relative to the main supernova peak. Our synthetic light curves of supernovae powered by magnetars transforming to black holes are consistent with those of some rapidly evolving bright transients recently reported by Arcavi et al. (2016).

Keywords: supernovae: general

1. INTRODUCTION

Some neutron stars (NSs) formed during the core collapse of massive stars are suggested to rotate very rapidly and, possibly for the same reason, to be strongly magnetized (Duncan & Thompson 1992; Mösta et al. 2015). These strongly magnetized, rapidly rotating NSs are often referred as "millisecond magnetars," although their connection–if any–to the high energy Galactic transients known also as magnetars is presently unclear. Millisecond magnetars possess a prodigious reservoir of rotational energy $\sim 10^{51}-10^{52}$ erg, which can be extracted during the first seconds to weeks after the explosion through electromagnetic dipole spin-down. If the energy from the magnetar wind is efficiently thermalized behind the expanding supernova (SN) ejecta shell (Metzger et al. 2014, see also Badjin 2016), then the resulting power source can greatly enhance the luminosity of the SN (e.g., Ostriker & Gunn 1971; Shklovskii 1976; Mazzali et al. 2006; Maeda et al. 2007).

Recent work on the magnetar model was motivated by the discovery of superluminous SNe (SLSNe)[1], events with peak luminosities greater than $\sim 10^{44}$ erg s^{-1}, i.e., more than an order of magnitude brighter than typical core-collapse SNe (Quimby et al. 2011; Gal-Yam 2012). For a surface magnetic dipole field strength of $\sim 10^{14}$ G and an initial rotational period of $\sim$ few ms, the magnetar releases sufficient rotational energy ($\gtrsim 10^{51}$ erg) over a proper timescale ($\sim 1-10$ days) to power SLSNe (Kasen & Bildsten 2010). Although magnetars provide one possible explanation for SLSNe (e.g., Kasen & Bildsten 2010; Woosley 2010; Dessart et al. 2012; Inserra et al. 2013; Metzger et al. 2014; Bersten et al. 2016; Sukhbold & Woosley 2016; Mazzali et al. 2016), several alternative models are also actively being explored (e.g., Moriya et al. 2010; Chevalier & Irwin 2011; Kasen et al. 2011; Chatzopoulos & Wheeler 2012a; Dessart et al. 2013; Kozyreva et al. 2014; Sorokina et al. 2015).

The growing number of well-sampled SLSN light curves (LCs) has revealed a rich diversity of behaviors. Some, and possibly all (Nicholl & Smartt 2016), SLSNe LCs show a "precursor bump" prior to the main peak (e.g., Leloudas et al. 2012; Nicholl et al. 2015a; Smith et al. 2016). This early maxima may be related to the existence of dense circumstellar media (CSM, Moriya & Maeda 2012), shock breakout from an unusually extended progenitor star (e.g., Piro 2015), or the interaction between the SN ejecta and the progenitor's companion star (Moriya et al. 2015).

Within the magnetar scenario, Kasen et al. (2016) show that precursor emission results naturally from the shock driven through the SN ejecta by the hot bubble inflated inside the expanding stellar ejecta by the magnetar wind (see also Bersten et al. 2016). If this "magnetar-driven" shock is strong enough, it becomes radiative near the stellar surface, powering an early LC bump. This emission component is distinct from the normal shock breakout signature from the SN explosion, which occurs at earlier times and is much less luminous due to the more compact initial size of the progenitor star.

[1] In this paper, we focus on Type Ic SLSNe and refer them as "SLSNe". Most Type II SLSNe are Type IIn SNe and their power source is likely the interaction between SN ejecta and dense circumstellar media (e.g., Moriya et al. 2013, but see also Inserra et al. 2016).

The extremely luminous transient ASASSN-15lh (Dong et al. 2016) also presents a challenge to SLSN models. The peak luminosity of ASASSN-15lh exceeds that of other SLSNe by about 1 magnitude, and its total radiated energy now exceeds 3×10^{52} erg (Godoy-Rivera et al. 2016; Brown et al. 2016). As this is near the maximum allowed rotational energy of a 1.4 $M_\odot$ NS, ASASSN-15lh was argued to challenge the magnetar model for SLSNe (Dong et al. 2016). However, Metzger et al. (2015) demonstrate that the maximum rotational energy increases with the NS mass, reaching $\approx 10^{53}$ erg for a NS close to the maximum observed mass of $\approx 2M_\odot$ for a range of nuclear equations of state consistent with measured NS masses and radii. Extremely luminous transients like ASASSN-15lh may indicate that some magnetars illuminating SNe can be very massive, although ASASSN-15lh itself may not only be explained by the magnetar model (e.g., Chatzopoulos et al. 2016) or may not even be a SLSN (Leloudas et al. 2016).

Slowly-rotating NSs can be supported against gravity only up to a maximum mass, which must exceed $\approx 2M_\odot$ but is otherwise poorly constrained (however, Ozel & Freire (2016) argue that this maximum mass is likely to be $\lesssim 2.2M_\odot$). Solid body rotation can stabilize NSs with masses up to $\approx 10\%$ higher than the maximum non-rotating mass for sufficiently rapid rotation. However, if the rotational energy of such *supramassive* NSs decreases below a critical minimum value ($E_{\rm coll}$), then the NS will collapse to a BH on a dynamical timescale (e.g., Shibata et al. 2000). Thus, if the magnetar produced in a core collapse SN has a mass in the supramassive range, and if it spins down to the point where its rotational energy becomes less than $E_{\rm coll}$, then it will suddenly collapse to a black hole (BH) and the central energy source powering the SN will suddenly cease. In this paper, we investigate the effect of the sudden termination of magnetar energy input due to BH transformation on the LCs of magnetar-powered SNe.

2. METHODS

2.1. *Energy input from magnetar spin-down*

We assume that the rotational energy of the central magnetar is emitted in a magnetized wind at the rate given by dipole vacuum or force-free spin-down (Ostriker & Gunn 1971; Contopoulos et al. 1999). The spin-down luminosity can be expressed as

$$L_{\rm mag}(t) = \frac{E_m}{t_m}\left(1+\frac{t}{t_m}\right)^{-2}, \quad (1)$$

where t is the time after the explosion, E_m is the initial rotational energy of the magnetar, and t_m is its spin-down timescale.

If the magnetar is supramassive and transforms to a BH after losing sufficient rotational energy, the central energy input from the magnetar suddenly ceases. From equation (1), the time of BH formation ($t_{\rm BH}$) is estimated to be

$$t_{\rm BH} = \frac{\Delta E}{E_{\rm coll}} t_m, \quad (2)$$

where $\Delta E \equiv E_m - E_{\rm coll}$. Thus, the central energy input from a supramassive magnetar can be expressed as

$$L_{\rm mag}(t) = \begin{cases} \frac{E_m}{t_m}\left(1+\frac{t}{t_m}\right)^{-2} & (t \le t_{\rm BH}), \\ 0 & (t > t_{\rm BH}). \end{cases} \quad (3)$$

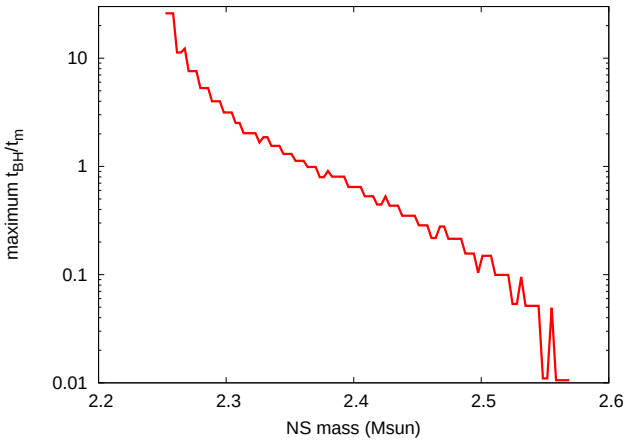

Figure 1. Maximum allowed ratio of BH formation time $t_{\rm BH}$ to magnetar spin-down time t_m, as a function of the NS gravitational mass, based on Figure 4 in Metzger et al. (2015). The structure of the solid-body rotating NS is calculated using the `rns` code (Stergioulas & Friedman 1995) assuming a parametrized piecewise polytropic EOS with an adiabatic index $\Gamma = 3$ above the break density of $\rho_1 = 10^{14.7}$ g cm^{-3} at a pressure of $P_1 = 3.2 \times 10^{34}$ dyn cm^{-2} (Margalit et al. 2015). The chosen EOS results in a 1.4 $M_\odot$ NS radius of 10.6 km and maximum non-rotating mass of ≈ 2.24 $M_\odot$, consistent with observational constraints.

Although we assume that central engine activity abruptly ceases after the BH transformation, ongoing fallback accretion to the BH may in some cases provide an additional ongoing source of energy (e.g., Dexter & Kasen 2013; Gilkis et al. 2016; Perna et al. 2016).

According to equation (2), there exists a maximum value of the ratio $t_{\rm BH}/t_m$ due to the maximum value of E_m which can be achieved for NSs of a given mass due to the mass-shedding limit (Metzger et al. 2015). Figure 1 shows the value of this maximum ratio as a function of the NS mass, based on Figure 4 of Metzger et al. (2015). Observe that $t_{\rm BH}/t_m$ becomes $\lesssim 1$ for NSs heavier than ~ 2.3 $M_\odot$. Such massive NSs, approaching the upper allowed supramassive range, transform to BHs before losing a significant amount of rotational energy.

2.2. *Light-curve calculations*

We employ the one-dimensional radiation hydrodynamics code STELLA for our numerical LC calculations (e.g., Blinnikov & Bartunov 1993; Blinnikov et al. 1998, 2006). STELLA implicitly treats time-dependent equations of the angular moments of intensity averaged over a frequency bin using the variable Eddington method. We adopt 100 frequency bins from 1 Å to 5×10^4 Å on a log scale. Local themodynamic equilibrium is assumed to determine the ionization levels of materials. The opacities of each frequency bin is evaluated by taking photoionization, bremsstrahlung, lines, and electron scattering into account. In particular, approximately 110 thousand lines in the list of Kurucz (1991) are taken into account for line opacities and they are estimated by using the approximation introduced in Eastman & Pinto (1993). See, e.g., Blinnikov et al. (2006) for more detailed description of the code.

Starting from the initial condition described below, we deposit energy from the magnetar spin-down at the center of the exploding star. We assume that the radiation energy from the magnetar is totally thermalized (Metzger et al. 2014), using $L_{\rm mag}(t)$ (Equation 3) directly as a source of thermal energy in STELLA (cf. Tominaga et al. 2013).

Table 1
Initial magnetar and SN ejecta properties of our synthetic models

model	NS mass $M_\odot$	E_m 10^{52} erg	t_m day	$E_{\rm coll}$ 10^{52} erg	$t_{\rm BH}$ day	$t_{\rm BH}/t_m$ $M_\odot$	$M_{\rm ej}$ $M_\odot$	^{56}Ni mass $M_\odot$
NS2p3m1	2.3	5.0	5	3.2	2.8	0.56	5	0.1
NS2p3m2	2.3	3.5	5	3.2	0.47	0.094	5	0.1
NS2p4m1	2.4	12.5	5	9.3	1.7	0.34	5	0.1
NS2p4m2	2.4	11	5	9.3	0.91	0.18	5	0.1
NS2p4m3	2.4	10	5	9.3	0.38	0.075	5	0.1
NS2p4m4	2.4	11	1	9.3	0.18	0.18	5	0.1
NS2p4m5	2.4	11	10	9.3	1.80	0.18	5	0.1
NS2p4m6	2.4	11	5	9.3	0.91	0.18	10	0.1
NS2p5m1	2.5	17.7	5	15.4	0.75	0.15	5	0.1
NS2p5m2	2.5	16	5	15.4	0.19	0.040	5	0.1

For comparison, we also show semi-analytic LC models from Arnett (1982), which is suitable for hydrogen-free SNe (cf. Valenti et al. 2008; Chatzopoulos et al. 2012b; Inserra et al. 2013). The semi-analytic LC is obtained by numerically integrating the following,

$$L(t) = \int_0^t 2\tau_m^{-2} L_{\rm mag}(t') t' e^{\left(\frac{t'-t}{\tau_m}\right)^2} dt'. \quad (4)$$

The effective diffusion time τ_m is expressed as

$$\tau_m = 1.05 \left(\frac{\kappa_e}{\beta c}\right)^{0.5} M_{\rm ej}^{0.75} E_{\rm ej}^{-0.25}, \quad (5)$$

where $M_{\rm ej}$ and $E_{\rm ej}$ are the total mass and kinetic energy, respectively, of the initial explosion. We assume κ_e = 0.1 cm^2 g^{-1} as the electron-scattering opacity of the SN ejecta and β = 13.8 (Arnett 1982).

2.3. *Initial SN ejecta properties*

We adopt a broken power-law structure for the initial density structure of the SN ejecta for simplicity, with a profile $\rho_{\rm ej} \propto r^{-\delta}$ at small radii which transitions to $\rho_{\rm ej} \propto r^{-n}$ outside of a break radius. Assuming homologous expansion of the SN ejecta ($r = v_{\rm ej} t$), we can express the initial density structure as (e.g., Chevalier & Soker 1989)

$$\rho_{\rm ej}(v_{\rm ej}, t) = \begin{cases} \frac{1}{4\pi(n-\delta)} \frac{[2(5-\delta)(n-5)E_{\rm ej}]^{(n-3)/2}}{[(3-\delta)(n-3)M_{\rm ej}]^{(n-5)/2}} t^{-3} v_{\rm ej}^{-n} & (v_{\rm ej} > v_t), \\ \frac{1}{4\pi(n-\delta)} \frac{[2(5-\delta)(n-5)E_{\rm ej}]^{(\delta-3)/2}}{[(3-\delta)(n-3)M_{\rm ej}]^{(\delta-5)/2}} t^{-3} v_{\rm ej}^{-\delta} & (v_{\rm ej} < v_t), \end{cases} \quad (6)$$

and

$$v_t = \left[\frac{2(5-\delta)(n-5)E_{\rm ej}}{(3-\delta)(n-3)M_{\rm ej}}\right]^{\frac{1}{2}}, \quad (7)$$

is the transitional velocity. We adopt n = 10 and δ = 1 as typical values (e.g., Matzner & McKee 1999). We adopt an initial value of $t = 10^3$ s in Eq. (6). The composition is assumed to be 50% carbon and 50% oxygen for simplicity.

In our fiducial model, we adopt typical properties for the SN ejecta in magnetar-powered SLSNe models of $M_{\rm ej} = 5\,M_\odot$ and $E_{\rm ej} = 10^{51}$ erg $\equiv$ 1 B (e.g., Nicholl et al. 2015b). We fix $E_{\rm ej} = 10^{51}$ erg in all the models, instead varying $M_{\rm ej}$ to investigate the effect of the SN ejecta on the LC properties (the effects of changing $M_{\rm ej}$ and $E_{\rm ej}$ are degenerate in the LC modeling). We also place 0.1 $M_\odot$ of the radioactive ^{56}Ni at the center of the SN ejecta, although it has little effect on early LCs.

3. LIGHT CURVES

3.1. *Effect of BH transformation*

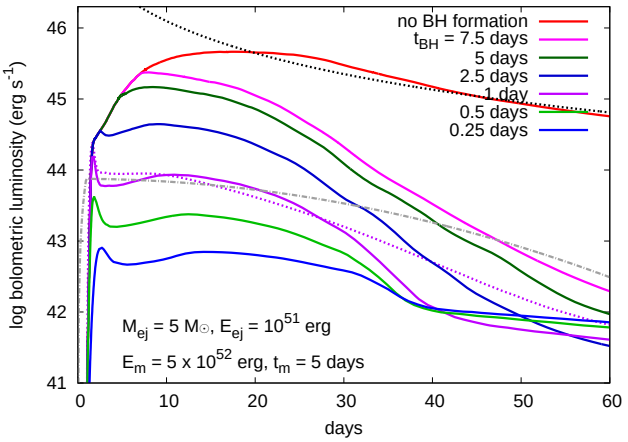

Figure 2. Bolometric LCs powered by magnetar spin-down. All the models have the same input parameters except for the BH transformation time ($t_{\rm BH}$). The solid lines are LC models obtained numerically and the dot-dashed line is the LC model obtained with the semi-analytic method assuming $t_{\rm BH}$ = 1 day. The dotted line near the semi-analytic model is the numerical LC model with $t_{\rm BH}$ = 1 day where the electron-scattering opacity is forced to be 0.1 cm^2 g^{-1}. The top dotted line is the input magnetar spin-down energy without BH formation.

Figure 2 shows a series of LCs corresponding to different NS collapse times, demonstrating the effect of BH formation on the LCs of magnetar-powered SNe. Other parameters, namely the initial rotational energy ($E_m = 5 \times 10^{52}$ erg), spin-down timescale (t_m = 5 days), and SN ejecta properties ($M_{\rm ej}$ = 5 $M_\odot$, $E_{\rm ej} = 10^{51}$ erg, and $M_{^{56}\rm Ni}$ = 0.1 $M_\odot$), are held fixed in the models in Figure 2.

The overall behavior of the LC evolution is reproduced reasonably well by the semi-analytic model, which in Figure 2 is shown by a dot-dashed line for the same magnetar luminosity input as for the $t_{\rm BH}$ = 1 day model. One difference between the numerical and semi-analytic models appears in the early rising part of the LC. While the semi-analytic model shows a continuous luminosity increase from day zero, the numerical model shows an early rise and maxima starting about 1 day after the explosion. This is the effect of the magnetar-driven shock breakout described by Kasen et al. (2016). Due to the large value of E_m released by supramassive NSs, the shock is strong and radiative, and the resulting magnetar-driven shock easily reaches the stellar surface. Figure 3 shows the hydrodynamic evolution of the numerical model, confirming that the shock breakout indeed occurs $\approx 0.5-1$ days after the explosion. Because the shock velocity is about 10000 km s^{-1} and the remaining distance from the shock to the surface is

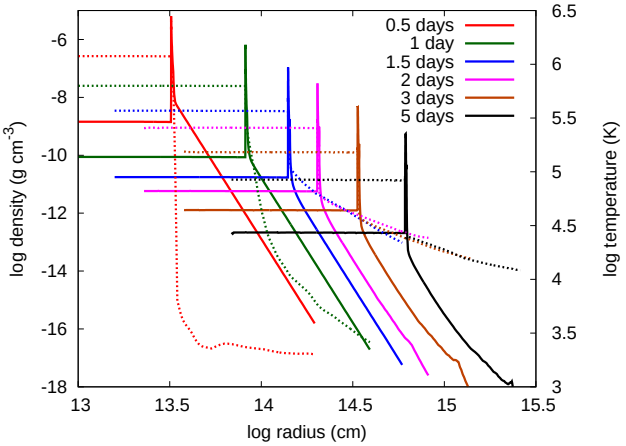

Figure 3. Hydrodynamic evolution of the numerical model with $t_{\rm BH}$ = 1 day in Figure 2. The shock breakout occurs at around 0.5 – 1 day after the explosion. The solid lines represent the density structure and the dotted lines show the temperature structure.

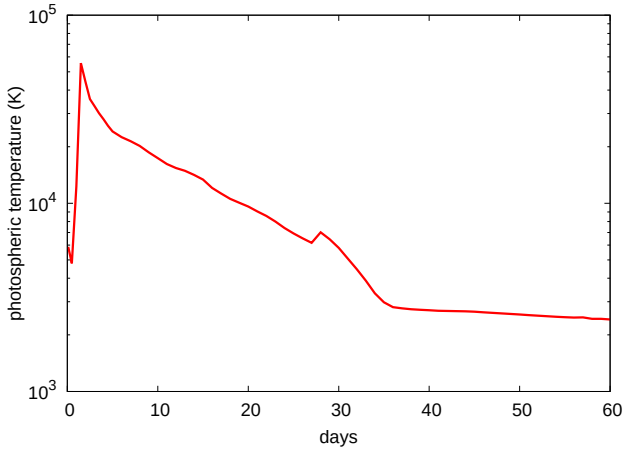

Figure 4. Photospheric temperature evolution of the numerical model with $t_{\rm BH}$ = 1 day shown in Figure 2.

about 10^{14} cm at the time of the shock breakout, the photon diffusion time above the shock is about 10^5 sec. Therefore, the LC reaches the first maxima at about 1 day after the shock breakout.

In general, the magnetar-driven breakout bump is more prominent in the LC in cases of early BH formation. This is due to the greater peak luminosity which, for a fixed value of the spin-down time t_m, increases with the magnetar lifetime. Although the luminosity contribution due to the direct diffusion of the spin-down power eventually comes to exceed that of shock breakout, the latter persists even after this time.

Kasen et al. (2016) also found that the suppression of the spin-down power is required to make the LC peak due to the magnetar-driven shock breakout prominent. Kasen et al. (2016) argued that the breakout peak can clearly appear if the thermalization of the spin-down energy from the magnetars is insufficient. In our model, the thermalization is kept efficient but the spin-down energy itself is shut down because of the BH transformation to make the LC peak prominent.

After the initial breakout peak, the numerical and semi-analytic LCs match reasonably well for some period of time. However, after $t \approx 20$ days the numerical LC begins to decline faster than the analytic expectation, presumably due to the effects of recombination and efficient adiabatic cooling in the SN ejecta. The semi-analytic model assumes a constant electron-scattering opacity of 0.1 cm^2 g^{-1}, which in reality will begin to decrease as the SN ejecta expand and cool due to recombination. For comparison, we show a numerical LC model with $t_{\rm BH}$ = 1 day where the electron-scattering opacity is forced to be 0.1 cm^2 g^{-1}. We can see that the numerical LC with 0.1 cm^2 g^{-1} declines slower than the actual numerical LC model, but they still decline faster than the semi-analytic model. The remaining difference likely comes from the more efficient adiabatic cooling in the numerical model with 0.1 cm^2 g^{-1} than the semi-analytic model. A part of the magnetar energy input is used to accelerate the SN ejecta in the numerical model and the kinetic energy of the SN ejecta is increased by the magnetar. Therefore, the adiabatic cooling is more efficient in the numerical model than in the semi-analytic model where no dynamical effect of the magnetar is taken into account. In the late phases, the numerical LC tracks the decay of ^{56}Co decay resulting from the initial 0.1 $M_\odot$ of ^{56}Ni.

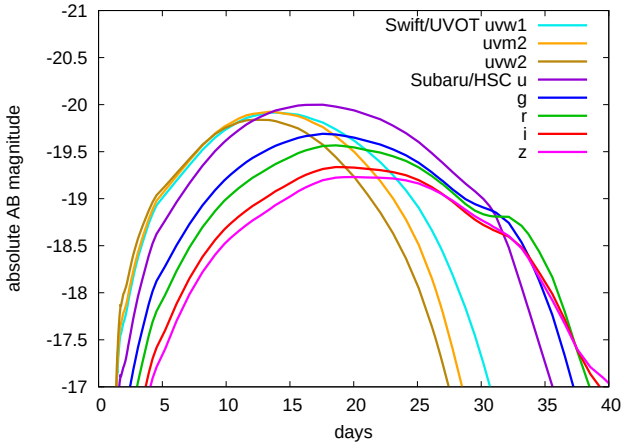

Figure 5. NUV and optical LCs of the numerical model with $t_{\rm BH}$ = 1 day shown in Figure 2.

Figure 4 shows the photospheric temperature evolution of the numerical model with $t_{\rm BH}$ = 1 day, while Figure 5 shows the near ultra-violet (NUV) and optical LC evolution of the same model. The multicolor LCs are obtained by convolving the filter functions of Swift/UVOT (*uvw*1, *uvm*2, and *uvw*2; Poole et al. 2008) and Subaru/HSC (*u*, *g*, *r*, *i*, and *z*; Miyazaki et al. 2012) with the spectral energy distribution obtained by STELLA. Although the early shock breakout bump is clearly visible in the bolometric LC, it does not contribute appreciably to the NUV and optical bands because of the very high photospheric temperature at the time of shock breakout. The high photospheric temperature also renders the NUV and optical LCs relatively faint. Although the bolometric luminosity reaches values of 10^{44} erg s^{-1} within the SLSNe range, the high photospheric temperature makes NUV and optical peak between –19 and –20 mag, below those of SLSNe.

3.2. *Parameter dependence*

The previous section addressed how the process of BH transformation for different formation times $t_{\rm BH}$ changes the LC properties of magnetar-powered SNe for fixed magnetar and SN ejecta properties. Here, we explore the effect of changing properties of the magnetar (NS mass, E_m, and t_m)

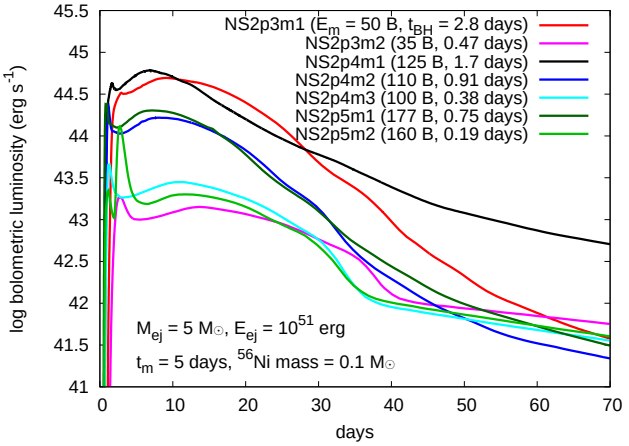
NS2p3m1 (E_m = 50 B, t_BH = 2.8 days)
NS2p3m2 (35 B, 0.47 days)
NS2p4m1 (125 B, 1.7 days)
NS2p4m2 (110 B, 0.91 days)
NS2p4m3 (100 B, 0.38 days)
NS2p5m1 (177 B, 0.75 days)
NS2p5m2 (160 B, 0.19 days)
M_ej = 5 M_⊙, E_ej = 10^51 erg
t_m = 5 days, 56Ni mass = 0.1 M_⊙
log bolometric luminosity (erg s^-1)
days

Figure 6. Numerical LC models with different initial magnetar properties and BH formation times. The initial conditions are summarized in Table 1.

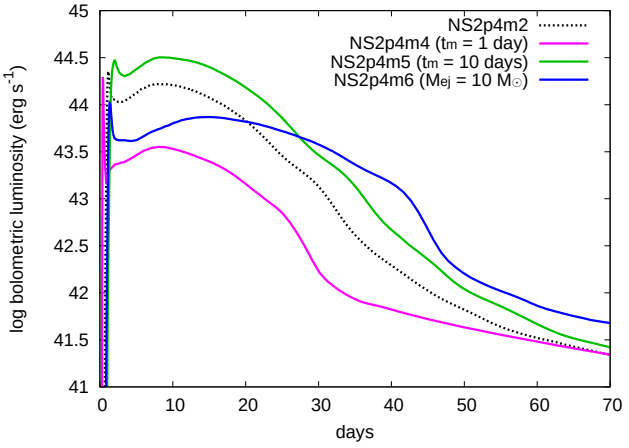

Figure 7. Numerical LC models with different SN ejecta and magnetar properties (see Table 1). The magnetar initial rotational energy ($E_m = 1.1 \times 10^{53}$ erg) and the NS mass (2.4 $M_\odot$, i.e., $E_{\rm coll} = 9.3 \times 10^{52}$ erg) are the same as those in NS2p4m2. The difference between NS2p4m2 ($M_{\rm ej} = 5\,M_\odot$, $E_{\rm ej} = 10^{51}$ erg, and $t_m = 5$ days) and the other models are indicated in the figure.

and the SN ejecta ($M_{\rm ej}$ and ^{56}Ni mass) within their physical ranges. For a given NS mass, there is the maximum value of E_m corresponding to the mass-shedding limit (e.g., Metzger et al. 2015), such that rotational energy E_m must lie in the range [$E_{\rm coll}$,max(E_m)]. Thus, once E_m and t_m are fixed, the value of $t_{\rm BH}$ is no longer a free parameter (cf. Eq. 2). We take these constraints into account in the models presented in this section, as summarized Table 1.

Figure 6 shows numerical LCs calculated for different E_m but fixing the value of t_m and the SN ejecta properties. Generally, the peak luminosity increases with higher E_m. However, both the values of $E_{\rm coll}$ and max(E_m) increase monotonically with the NS mass. For NS with masses approaching the maximum range of supramassive NSs, the values of max(E_m) and $E_{\rm coll}$ become sufficiently close that the NS collapses to a BH before releasing the significant amount of the rotational energy. Extremely massive magnetars do not therefore produce bright SNe, despite the large rotational energy

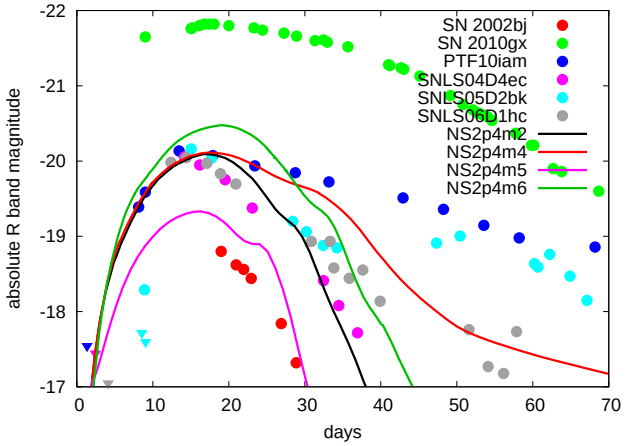

Figure 8. Comparison between the synthetic *R*-band LCs and rapidly-evolving bright transients. We show the LCs of SN 2002bj (Poznanski et al. 2010), a typical rapidly declining SLSN (SN 2010gx, Pastorello et al. 2010), and the Arcavi transients (PTF10iam, SNLS04D4ec, SNLS05D2bk, and SNLS06D1hc, Arcavi et al. 2016). The triangles in the figure indicate the upper limits of the observations.

E_m available.[2] The maximum peak luminosity we obtain is around 10^{45} erg s^{-1}, which are powered by the NSs of mass $\lesssim 2.5\,M_\odot$ for the assumed equation of state (Fig. 6). The peak luminosity ranges between 10^{43} erg s^{-1} and 10^{45} erg s^{-1} in our models.

Figure 7 shows the numerical LCs for a fixed value of $E_m = 1.1 \times 10^{53}$ erg but varying the spin-down time t_m and the SN ejecta properties. Because $t_{\rm BH}/t_m$ is fixed for a given value of E_m and $E_{\rm coll}$, then the value of $t_{\rm BH}$ decreases with t_m. Magnetars with shorter spin-down times t_m result in smaller peak luminosities because the BH transformation occurs earlier, such that most of the magnetar energy is lost to PdV expansion instead of being released as radiation. Models with a larger ejecta mass $M_{\rm ej}$ results in the longer LC duration because of the longer diffusion time, as expected.

4. DISCUSSION

4.1. *Comparison with observations*

Figure 8 compares our synthetic *R*-band LCs to the measured LCs of rapidly-evolving luminous transients. As previously discussed, the optical luminosity of the synthetic LCs are relatively faint compared to the bolometric luminosity because of the high photospheric temperature. The peak luminosities of our models are typically between –20 and –21 mag. Therefore, our transients are brighter than most core-collapse SNe, yet fainter than typical SLSNe. Arcavi et al. (2016) recently reported transients precisely within this luminosity range, some of which show similar LC behavior to those predicted by our model. Although the peak luminosities of the Arcavi transients can be explained by magnetars of typical masses with the initial spin of a few ms and the magnetic field strength of $\sim 10^{15}$ G, Arcavi et al. (2016) found that the overall rapid LC evolution is hard to be explained by the magnetar model. However, we accomplished the rapid evolution by shutting down the magnetar power by the BH transformation. The rapid LC evolution in our models is also consistent with that of SN 2002bj (Poznanski et al. 2010).

[2] The remaining rotational energy is ultimately trapped in the spin of the BH.

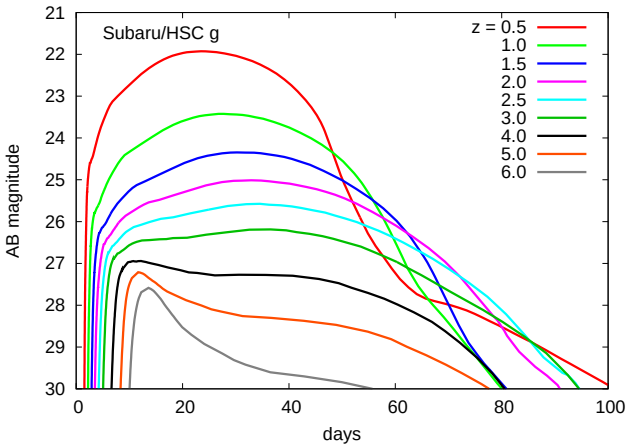

Figure 9. Redshifted LCs of the model with t_m = 1 day in Fig. 2 observed with the *g* band of Subaru/HSC.

If the Arcavi et al. (2016) events and SLSNe are both powered by magnetars, then one might assume that they should occur in similar host galaxies. However, the Arcavi transients occur in relatively higher metallicity environments than SLSNe, which instead prefer low metallicity (e.g., Chen et al. 2016b; Perley et al. 2016; Leloudas et al. 2015; Lunnan et al. 2015). On the other hand, normal SLSNe are likely powered by less massive, stable magnetars, while the magnetars described in this work are necessarily very massive. Core collapse explosions giving rise to different NS masses could in principle map to different progenitor environments. Alternatively, the Arcavi transients may have several distinct origins, including those powered by magnetars transforming to BHs, and thus could originate from a diversity of environments.

We have focused on the magnetars with the spin-down timescales of the order of days which correspond to the magnetic field strengths of $\sim 10^{14}$ G. Their spin-down timescales can be shorter (seconds or less) with stronger magnetic fields and such magnetars can be progenitors of, e.g., gamma-ray bursts (GRBs) (e.g., Metzger et al. 2015). The BH transformation can also occur in such magnetars possibly affecting the observational properties of GRBs, but this is beyond the scope of this paper.

4.2. *Observing the magnetar-driven shock breakout bump*

Although the signature of magnetar-driven shock breakout is clearly visible in our bolometric LCs, they are difficult to observe in optical bands because of their high photospheric temperature and short duration. However, optical surveys could detect them more readily at high redshifts due to *K*-correction and time dilation effects. Figure 9 shows the LCs of SN powered by magnetars transforming to BHs as observed at redshifts $z = 0.5-6$ in the *g* band of Subaru/HSC.

The flat LC becomes visible after the initial LC rise for events at $z \gtrsim 2$, while a clear shock breakout bump appears only at $z \gtrsim 5$. Unfortunately, a transient survey with a depth of 28 mag would be required to detect the bump in this case. However, depending on the initial properties of the magnetar and the SN ejecta, the bump may become brighter than assumed in our fiducial models, in which case detection might still be feasible by deep transient surveys by instruments like LSST or Subaru/HSC with a proper cadence (Tanaka et al. 2012).

5. CONCLUSIONS

We have investigated the observational properties of SNe powered by temporarily stable supramassive magnetars which transform to BHs following a brief spin-down phase. This sudden collapse to a BH results in an abrupt cessation of energy input from the central engine. Our LC modeling of such transients have shown that their LCs decline much quicker than those of SN powered by the indefinitely stable, lower mass magnetars, which are usually invoked as the engines of SLSNe.

We also find that the magnetar-driven shock breakout signal can be more significant in SNe powered by magnetars transforming to BHs, due in part to the higher rotational energy of a massive NS and the fact that prompt BH formation can allow the breakout signal to more readily shine above the normal spin-down powered LC. Unfortunately, this breakout signal is not readily visible in NUV or optical wavebands because of the high photospheric temperature at early times. Nevertheless, such a breakout signal could be more readily detected in optical at high redshifts, or at low redshifts by future wide-field UV transient surveys. The multi-dimensional effects like Rayleigh-Taylor instabilities in the shell causing the magnetar-driven shock breakout (e.g., Chen et al. 2016a) may also affect the shock breakout signatures. Our synthetic LCs of short-lived magnetars appear to be consistent with some of the rapidly-evolving bright transients recently reported by Arcavi et al. (2016).

We thank the anonymous referee for the comments that improved this paper. TJM is supported by the Grant-in-Aid for Research Activity Start-up of the Japan Society for the Promotion of Science (16H07413). BDM gratefully acknowledges support from NASA grants NNX15AU77G (Fermi), NNX15AR47G (Swift), and NNX16AB30G (ATP), and NSF grant AST-1410950, and the Alfred P. Sloan Foundation. The work of S.Blinnikov on development of STELLA code is supported by Russian Science Foundation grant 14-12-00203. Numerical computations were partially carried out on the PC cluster at Center for Computational Astrophysics, National Astronomical Observatory of Japan.

REFERENCES

Arcavi, I., Wolf, W. M., Howell, D. A., et al. 2016, ApJ, 819, 35
Arnett, W. D. 1982, ApJ, 253, 785
Badjin, D. A. 2016,
http://wwwmpa.mpa-garching.mpg.de/hydro/NucAstro/PDF_16/Badj
Bersten, M. C., Benvenuto, O. G., Orellana, M., & Nomoto, K. 2016, ApJL, 817, L8
Blinnikov, S. I., & Bartunov, O. S. 1993, A&A, 273, 106
Blinnikov, S. I., Eastman, R., Bartunov, O. S., Popolitov, V. A., & Woosley, S. E. 1998, ApJ, 496, 454
Blinnikov, S. I., Röpke, F. K., Sorokina, E. I., et al. 2006, A&A, 453, 229
Brown, P. J., Yang, Y., Cooke, J., et al. 2016, ApJ, 828, 3
Chatzopoulos, E., & Wheeler, J. C. 2012a, ApJ, 760, 154
Chatzopoulos, E., Wheeler, J. C., Vinko, J., et al. 2016, arXiv:1603.06926
Chatzopoulos, E., Wheeler, J. C., & Vinko, J. 2012b, ApJ, 746, 121
Chatzopoulos, E., Wheeler, J. C., Vinko, J., Horvath, Z. L., & Nagy, A. 2013, ApJ, 773, 76
Chen, K.-J., Woosley, S. E., & Sukhbold, T. 2016a, arXiv:1604.07989
Chen, T.-W., Smartt, S. J., Yates, R. M., et al. 2016b, arXiv:1605.04925
Chevalier, R. A., & Irwin, C. M. 2011, ApJL, 729, L6
Chevalier, R. A., & Soker, N. 1989, ApJ, 341, 867
Contopoulos, I., Kazanas, D., & Fendt, C. 1999, ApJ, 511, 351
Dessart, L., Hillier, D. J., Waldman, R., Livne, E., & Blondin, S. 2012, MNRAS, 426, L76
Dessart, L., Waldman, R., Livne, E., Hillier, D. J., & Blondin, S. 2013, MNRAS, 428, 3227
Dexter, J., & Kasen, D. 2013, ApJ, 772, 30
Dong, S., Shappee, B. J., Prieto, J. L., et al. 2016, Science, 351, 257
Duncan, R. C., & Thompson, C. 1992, ApJL, 392, L9

Eastman, R. G., & Pinto, P. A. 1993, ApJ, 412, 731
Gal-Yam, A. 2012, Science, 337, 927
Gilkis, A., Soker, N., & Papish, O. 2016, ApJ, 826, 178
Godoy-Rivera, D., Stanek, K. Z., Kochanek, C. S., et al. 2016, arXiv:1605.00645
Inserra, C., Smartt, S. J., Gall, E. E. E., et al. 2016, arXiv:1604.01226
Inserra, C., Smartt, S. J., Jerkstrand, A., et al. 2013, ApJ, 770, 128
Kasen, D., & Bildsten, L. 2010, ApJ, 717, 245
Kasen, D., Woosley, S. E., & Heger, A. 2011, ApJ, 734, 102
Kasen, D., Metzger, B. D., & Bildsten, L. 2016, ApJ, 821, 36
Kozyreva, A., Blinnikov, S., Langer, N., & Yoon, S.-C. 2014, A&A, 565, A70
Kurucz, R. L. 1991, NATO Advanced Science Institutes (ASI) Series C, 341, 441
Leloudas, G., Chatzopoulos, E., Dilday, B., et al. 2012, A&A, 541, A129
Leloudas, G., Fraser, M., Stone, N. C., et al. 2016, arXiv:1609.02927
Leloudas, G., Schulze, S., Krühler, T., et al. 2015, MNRAS, 449, 917
Lunnan, R., Chornock, R., Berger, E., et al. 2015, ApJ, 804, 90
Maeda, K., Tanaka, M., Nomoto, K., et al. 2007, ApJ, 666, 1069
Margalit, B., Metzger, B. D., & Beloborodov, A. M. 2015, Physical Review Letters, 115, 171101
Matzner, C. D., & McKee, C. F. 1999, ApJ, 510, 379
Mazzali, P. A., Deng, J., Nomoto, K., et al. 2006, Nature, 442, 1018
Mazzali, P. A., Sullivan, M., Pian, E., Greiner, J., & Kann, D. A. 2016, MNRAS, 458, 3455
Metzger, B. D., Margalit, B., Kasen, D., & Quataert, E. 2015, MNRAS, 454, 3311
Metzger, B. D., Vurm, I., Hascoët, R., & Beloborodov, A. M. 2014, MNRAS, 437, 703
Miyazaki, S., Komiyama, Y., Nakaya, H., et al. 2012, Proc. SPIE, 8446, 84460Z
Moriya, T. J., Blinnikov, S. I., Tominaga, N., et al. 2013, MNRAS, 428, 1020
Moriya, T. J., Liu, Z.-W., Mackey, J., Chen, T.-W., & Langer, N. 2015, A&A, 584, L5
Moriya, T. J., & Maeda, K. 2012, ApJL, 756, L22
Moriya, T., Tominaga, N., Tanaka, M., Maeda, K., & Nomoto, K. 2010, ApJL, 717, L83
Mösta, P., Ott, C. D., Radice, D., et al. 2015, Nature, 528, 376
Nicholl, M., & Smartt, S. J. 2016, MNRAS, 457, L79
Nicholl, M., Smartt, S. J., Jerkstrand, A., et al. 2015a, ApJL, 807, L18
Nicholl, M., Smartt, S. J., Jerkstrand, A., et al. 2015b, MNRAS, 452, 3869
Ostriker, J. P., & Gunn, J. E. 1971, ApJL, 164, L95
Ozel, F., & Freire, P. 2016, arXiv:1603.02698
Pastorello, A., Smartt, S. J., Botticella, M. T., et al. 2010, ApJL, 724, L16
Perley, D. A., Quimby, R., Yan, L., et al. 2016, arXiv:1604.08207
Perna, R., Lazzati, D., & Giacomazzo, B. 2016, ApJL, 821, L18
Piro, A. L. 2015, ApJL, 808, L51
Poole, T. S., Breeveld, A. A., Page, M. J., et al. 2008, MNRAS, 383, 627
Poznanski, D., Chornock, R., Nugent, P. E., et al. 2010, Science, 327, 58
Quimby, R. M., Kulkarni, S. R., Kasliwal, M. M., et al. 2011, Nature, 474, 487
Shibata, M., Baumgarte, T. W., & Shapiro, S. L. 2000, Phys. Rev. D, 61, 044012
Shklovskii, I. S. 1976, Soviet Ast., 19, 554
Smith, M., Sullivan, M., D'Andrea, C. B., et al. 2016, ApJL, 818, L8
Sorokina, E., Blinnikov, S., Nomoto, K., Quimby, R., & Tolstov, A. 2015, arXiv:1510.00834
Stergioulas, N., & Friedman, J. L. 1995, ApJ, 444, 306
Sukhbold, T., & Woosley, S. E. 2016, ApJL, 820, L38
Tanaka, M., Moriya, T. J., Yoshida, N., & Nomoto, K. 2012, MNRAS, 422, 2675
Tominaga, N., Blinnikov, S. I., & Nomoto, K. 2013, ApJL, 771, L12
Valenti, S., Benetti, S., Cappellaro, E., et al. 2008, MNRAS, 383, 1485
Woosley, S. E. 2010, ApJL, 719, L204